IIETA International Information and Engineering Technology Association
Advancing the World of Information and Engineering

Journal of New Materials for Electrochemical Systems
Vol. 27, No. 4, December 2024, pp. 324-339
Journal homepage: http://iieta.org/journals/jnmes

# Power Quality Enhancement Using Artificial Neural Network-Proportional Integral Controller and Fuzzy Granular Controller for DSTATCOM Integrated with Renewable Energy and Battery Storage System

Peram Venkata Ramana[1*], K. Mercy Rosalina[2]

[1] Research Scholar, Vignan's Foundation for Science, Technology and Research, Guntur 522002, India
[2] Professor, Vignan's Foundation for Science, Technology and Research, Guntur 522002, India

Corresponding Author Email: 211fg06203@vignan.ac.in

Copyright: ©2024 The author(s). This article is published by IIETA and is licensed under the CC BY 4.0 license (http://creativecommons.org/licenses/by/4.0/).

https://doi.org/10.14447/jnmes.v27i4.a04

**Received:** June 12, 2024
**Accepted:** September 28, 2024

***Keywords:***
*Distributed static compensator (DSTATCOM), Artificial neural network (ANN), Proportional-Integral (PI), Fuzzy granular, permanent magnet synchronous generator (PMSG), Wind energy conversion system (WECS)*

## ABSTRACT

In the power distribution network, spread of power electronic devices and nonlinear loads has been exacerbate the power quality (PQ) difficulties. D-STATCOMs plays a key role to serve as an active power filter which are commonly used to address these issues. The performance of the distribution network is increased by incorporating the renewable energy sources (RES) such as PMSG- based wind energy conversion system (WECS) with DC capacitor across the D-STATCOM. During the PQ disturbances without controller the THD of source and load currents are 7.46% and 15.32%, by using the PI controller THD's are reduced to 3.02% and 4.01%. The proposed controllers reduced THD with ANN-PI source and load current THD are 2.99% and 3.62% and Fuzzy granular controller are 1.56% and 2.37%. Whereas on the other side, the DC-link voltage with PI controller introduces more fluctuations and reduced voltage level with settling time about 0.1secs, by using ANN-PI voltage fluctuations get reduced and maintain constant voltage, in addition to that in fuzzy granular the magnitude of dc link voltage increased by 10% and settling time got reduced about 0.05secs. The non-sinusoidal source current and load current are tranformed to sinusiodal by the ANN-PI and Fuzzy granular controller and also the power factor is improved nearly to unity. The proposed controllers are designed and tested by using MATLAB/Simulink.

## NOMENCLATURE

| | |
|---|---|
| $V_1$ (or)$V_{PMSG}$ | WECS-PMSG Voltage |
| $V_2$ | Voltage Across the Capacitor |
| $V_3$ | Voltage Across the Load |
| $i_{PMSG}$ | PMSG Current |
| $d_1, d_2, d_3$ | Duty Cycles of The IGBT Switches in The MPPT Boost Converter |
| $T_{sw}$ | Switching Time Constant |
| $\Delta I_{L1max}$ | Maximum Ripple Current |
| $P_{PMSG}$ | WECS-PMSG Real Power |
| $K_a$ | Attenuation Factor |
| $\omega_{res}$ | Angular Resonance Frequency |
| $V_{20}$ | Initial Bus Voltage of the WECS-PMSG- MPPT |
| $I_{BESS, err}^*$ | Battery current error |
| $I_{BESS}$ | BESS Charging and Discharging Current |
| $_{iL1}^*$ | Reference Current of Inductor Boost Converter |
| $i_{L1}$ | Boost Converter Current |
| $K_{pi}$ | Proportional Gain |
| $K_{ii}$ | Integral Gain |
| $G_{PI}(s)$ | Current-Tuned Proportional-Integral Controller |
| $G_{sw}(s)$ | Offset Switching Frequency Block |
| $P_{grid}$ | DC-Link Real Power |
| $G_{PMSG}(s)$ | Transfer Function of WECS-PMSG System |
| $\omega_n$ | Undammed Frequency |
| $G_{olimit}(s)$ | Transfer Function of Limitations on the MPPT |
| $G_{omppt}$ | Output Transfer Function of The MPPT |
| $V_2^*$ | Reference Dc Link Voltage |
| $I_{ref, dc}$ | Reference Current for The Battery |
| $I_{grid, out}$ | Output Grid Current |
| $V_{dc, err}$ | DC link voltage error |

## ACRONYMS

| | |
|---|---|
| ANN | Artificial Neural Network |
| PI | Proportional Integral |
| PMSG | Permanent Magnet Synchronous Generator |
| MPPT | Maximum Power Point Tracking |
| VCM | Voltage Control Mode |
| PFCM | Power Factor Control Mode |
| LPF | Low Pass Filter |

| | | | |
|---|---|---|---|
| WECS | Wind energy conversion system | PCC | Point of Common Coupling |
| PQ | Power Quality | FLC | Fuzzy Logic Controller |
| BESS | Battery Energy Storage system | SOC | State of Charge |
| DSTATCOM | Distributed Static Compensator | LMBP | Levenberg-Marquardt Back Propagation |
| SMC | Sliding Mode Control | MF | Membership Function |

## 1. INTRODUCTION

The growing usage of power electronic devices in modern drives, appliances, and other loads has resulted in a large increase in nonlinear loads throughout distribution networks. The main source of harmonic distortion, which can reduce power quality (PQ) and negatively impact the operation [1] of utility equipment, is these nonlinear loads. Active power filtering has been shown to mitigate the adverse effects of PQ issues. Distributed static compensators, or DSTATCOMs, can help fix PQ problems in distribution networks [2]. DSTATCOMs function as shunt active power filters by regulating voltage and compensating for harmonics via a shared DC link [3]. In recent advances, distribution networks have seen the synergistic integration of PMSG-based Wind Energy Conversion Systems (WECS) and Distribution Static Compensators (DSTATCOMs) into distribution networks [3-4]. Power quality (PQ) is simultaneously improved and renewable energy sources are seamlessly integrated with this integrated method [5]. DSTATCOM control techniques have been the subject of several studies. Proportional-integral (PI) controllers with Park's and Clarke's transformations are used in traditional approaches [6]. DSTATCOM performance is being enhanced by AI techniques like Fuzzy Logic Control and Artificial Neural Networks (ANNs) [7-8]. These changes are intended to provide better power factor correction, more stringent harmonic current control, and steady DC-link voltage management [9].

A unique control strategy that integrates essential approaches could be advantageous for DSTATCOM capacitor voltage regulators. These techniques yield a DC-link voltage that is steady, has a quick response time, little settling time, and minimal overshoot [11]. Intelligent controllers such as Fuzzy, ANN, and Evolutionary Search have been used to study power factor correction methods, harmonic removal, and Total Harmonic Distortion (THD) analysis for PI controller tuning. Moreover, DSTATCOM integration with microgrids has been investigated as a means of resolving PQ issues resulting from fluctuating loads. Research has examined DSTATCOMs' THD performance in steel mills with induction furnace loads [12]. Lastly, research has focused on creating sophisticated controllers to lessen grid voltage distortions and THD, such as SMC and hybrid approaches. This study illustrates system limitations and expands upon DSTATCOM control research. For dynamic load variations, conventional techniques based on Park's and Clarke's transformations with PI controllers might not be appropriate. Moreover, the integration of renewable energy sources with DSTATCOMs has not received much attention in the current study. This research presents new control strategies for a DSTATCOM combined with a PMSG-WECS system. By addressing the aforementioned constraints, these control strategies aim to enhance DSTATCOM performance in distribution networks that have a significant amount of renewable energy sources and nonlinear loads. The Permanent Magnet Synchronous Generator and Distributed Static Compensator (DSTATCOM) are the two components of this wind energy conversion machine. The DSTATCOM eliminates unwanted harmonic currents from the supply to control power quality. This type of VSC is connected to the DC-Link capacitor in simultaneously.

Reactive power via DC-Link and AC is controlled by it. ANNs are computational models inspired by biological neural networks [10]. The ANN is trained to adjust the shunt VSC control signals in order to maintain a steady DC-Link capacitor voltage [11]. Fuzzy granular [13] and ANN-PI[ 12] are employed in this work in a similar manner to traditional PI controllers their functions and advantages are discussed. Nevertheless, ANN-PI and Fuzzy granular are improved to satisfy the theme criteria and are discussed.
This work specifically contributes to:

- The source side voltage and current will also be compensated since the load side voltages and currents are efficiently compensated using the DSTATCOM-PMSG-WECS utilizing various advanced controllers.
- The creation of a hybrid fuzzy mode control technique to ensure effective use of the wind power that is available for the PMSG-WECS system's maximum power point tracking (MPPT).
- In order to lower Total Harmonic Distortion (THD), improve power factor, diminish grid voltage fluctuations, and control DC-link voltage with a short settling time, DSTATCOM-PMSG employs a modified ANN-PI.
- Fuzzy granular approach reduces total harmonic distortion (THD) on the load and source sides of the distribution network, which enhances the voltage waveform.
- Examined the DSTATCOM-WECS system under different supply and loading conditions. The effectiveness of the system will be evaluated using voltage and current waveform representations, power factor, and THD.

## 2. CONFIGURATION OF PROPOSED TOPOLOGY

The proposed DSTATCOM combined with a PMSG-based WECS for a three-phase distribution network is configured as shown in Figure 1. A boost converter connects the WECS-PMSG to the DSTATCOM's DC-link [7]. The distribution network serves as an active power filter and is shunt connected to the DSTATCOM. It interfaces with the grid using a combination of capacitance, inductance, and resistance to accomplish this capability. With this setup, compensatory currents can be injected into the network by the DSTATCOM to reduce settling time and mitigate current harmonics while maintaining DC-link voltage.

The proposed system uses a PMSG-based WECS in a three-phase distribution network in conjunction with a DSTATCOM configured as a shunt voltage source converter (VSC). A boost converter links the WECS-PMSG [16] to the DC-link of the DSTATCOM, as shown in Figure 1. This configuration makes use of the DSTATCOM's ability to function as an active power filter by combining resistance, inductance, and capacitance to interact with the grid. By purposefully injecting compensating currents, the

DSTATCOM lessens the impacts of current harmonics and keeps the DC-link voltage stable with short settling times.

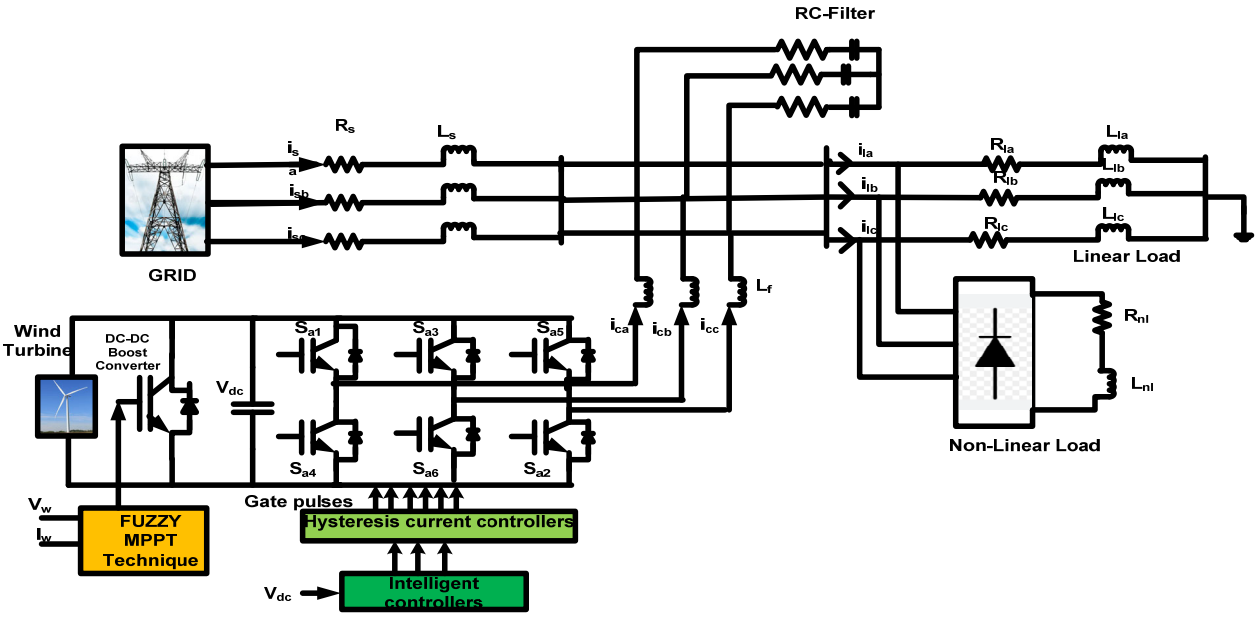


**Figure 1:** Configuration of the System

## 2.1 External support for DC-link

A configuration with a WECS-PMSG as the source feeding power into a shared DC-link is shown in Figure 2. Additionally, a DSTATCOM and a PMSG-based WECS system are connected to this DC-link. The DC-link has a shared capacitor that serves the WECS and the DSTATCOM.

The different parts of the system are connected by a common DC bus. It makes it easier for electricity to move between the DG unit, WECS, DSTATCOM, and maybe the grid (based on the exact arrangement). In order to enhance power quality, the DSTATCOM acts as a shunt active power filter by introducing compensatory currents into the grid. In order to perform its function, it uses electricity from the DC-link [17]. The Permanent Magnet Synchronous Generator (PMSG) is the most important component of the Wind Energy Conversion System (WECS)[15]. Wind energy is transformed into mechanical energy and used to produce electricity. The shared DC-link receives the DC output from the PMSG. As it stores and releases energy as needed, this capacitor is an essential component of the system. It assists in preserving a steady DC voltage level inside the DC-link, which is essential to the DSTATCOM and WECS operating well.

The potential of the DSTATCOM to function as an active power filter. By purposefully injecting compensating currents, the DSTATCOM lessens the impacts of current harmonics and keeps the DC-link voltage stable with short settling times. When the grid voltage is healthy and the load is balanced, the WECS-PMSG [20] charges the capacitor by providing DC power to the DC-link. The DSTATCOM then injects compensatory currents into the grid as necessary to preserve power quality. When there is an imbalanced load, the DSTATCOM actively controls the currents going to each phase to guarantee that the load receives balanced power supply even while the incoming power is unbalanced.

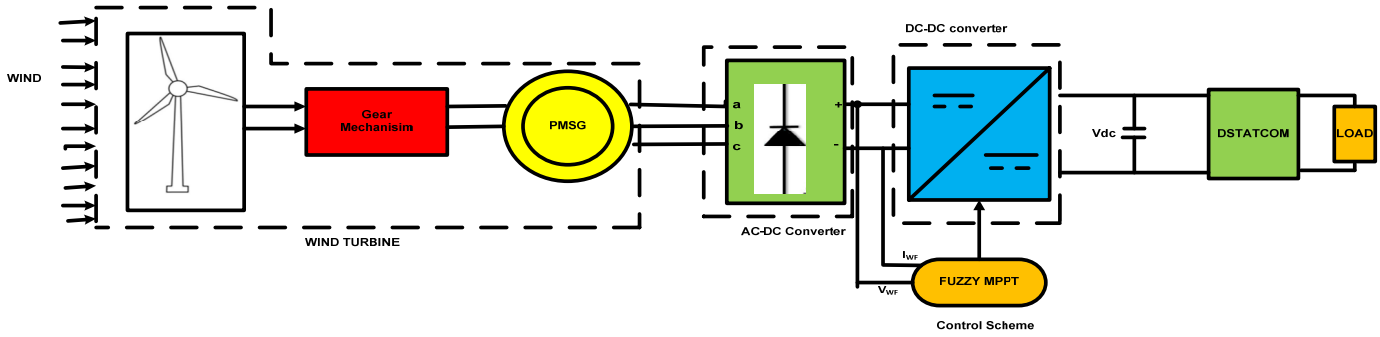


**Figure 2:** Distributed generation fed DC-Link for DSTATCOM

The WECS-PMSG is directly connected to the DC-link due to the presence of an inverter between the PMSG and the DC-link. Depending on the control method used, this design provides greater control over the DC voltage level and may allow for bidirectional power flow between the WECS and the grid. The inverter turns the PMSG's AC output into DC voltage. The wind turbine drives the PMSG, which provides alternating current electricity. The AC filter removes high-frequency components and harmonics from the PMSG output. The inverter transforms the filtered AC voltage from the PMSG to DC voltage. This DC voltage is delivered into the DC-link capacitor. The DC energy from the WECS-PMSG is stored in the DC-link capacitor. The DC energy flowing from the capacitor is managed by the DSTATCOM inverter. When

necessary, it injects compensating currents into the grid to address power quality concerns by converting the DC voltage into a regulated AC voltage waveform.

As illustrated in Figure 3, the suggested system makes use of three main control strategies: a traditional PI [26] controller for the DSATCOM for Power Quality Enhancement functions as a shunt active filter for power factor enhancement and voltage harmonic reduction. When there are any grid-related disturbances on the source side, it will function as a shunt voltage compensator. Without the need for any switching operations, all of these configurations will run automatically.

- Voltage Control Mode (VCM): By controlling the reactive current component, VCM maintains voltage at the Point of Common Coupling (PCC). Reactive current is adjusted in accordance with the comparison between the observed PCC voltage and a reference. Reactive current-proportional voltage change is possible with a droop control system.
- Power Factor Control Mode (PFCM): By setting the reactive power reference to the measured reactive power of the wind production, PFCM ensures unity power factor. This guarantees that the wind turbine will receive all of the reactive power needed from the system.
- The reference active power is computed by taking as inputs the desired regulation power and the amount of measured active power by the wind turbine. Steady-state faults in the active current reference are removed using a PI controller. As shown in Figure 3, the Inner Current Control Loop guarantees decoupled control of the direct and quadrature current components (id and iq). These currents are regulated by PI controllers using feedback from the DSTATCOM output.
- The grid functions as a DC voltage regulator, and a separate PI controller controls the DC voltage on the DC bus by trading a tiny quantity of active power. The control system controls the DC voltage inside the DSTATCOM, maintains power quality at the PCC, and guarantees effective power flow.

## 3. WECS PMSG SYSTEM WITH COMMON DC-LINK CONNECTED DSTATCOM

An analytical model of the WECS-PMSG-DSTATCOM system coupled to a shared DC link is presented in this section. First, we go over the block diagram representation of the WECS-PMSG system in mathematics. Next, we obtain the dynamic equations for the DC link, encompassing its constituents, switching architecture, and the behaviour of current and voltage. Furthermore, the output voltage equation derivation with a PI controller is provided. Lastly, additional details on the block diagram representation are provided, including the modelling of the PI controller, the operation of the buck-boost converter using transfer function analysis, and the WECS-PMSG-DSTATCOM system with the MPPT controller.

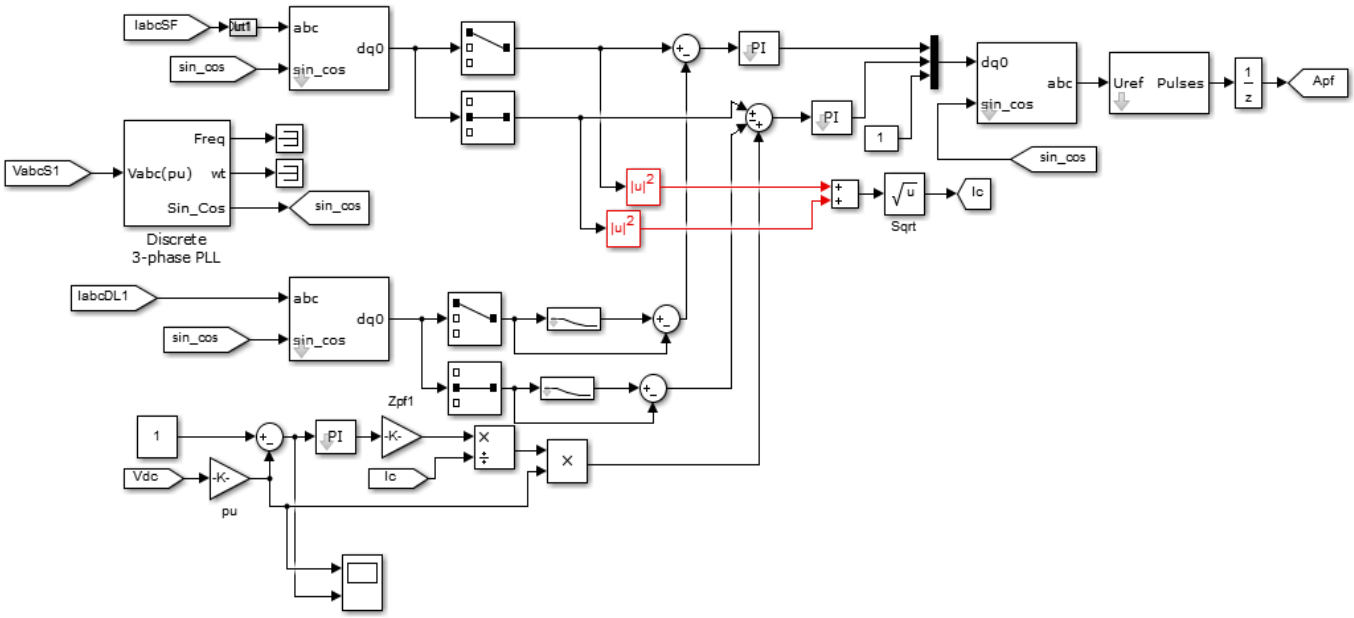


**Figure 3:** WECS-PMSG with DC-DC buck-boost controller

### 3.1 Modeling of WECS-PMSG-DSTATCOM system

In order to provide a steady and reliable power supply, a WECS-PMSG-DSTATCOM electrical power generation system is normally supported by a common dc-link capacitor voltage [21]. This WECS-PMSG system's MG can be hybrid AC/DC or ac to dc. An MPPT boost converter, battery bank, dual-direction DC-DC converter coupled to a common DC link terminal, and buck converter for the load connection are all included in this topology, which is made up of subsystems such as WECS-PMSG-DSTATCOM. In order to extract maximum power from the wind subsystem, the maximum power point tracking (MPPT) [19] technique uses dc voltage stepping up. This technique helps to extract continuous voltage from the WECS-PMSG cell and maintain a steady D.C output. The input voltage V1 and current i1 are received by the WECS-PMSG-DSTATCOM MPPT cell and are then increased by a switch, diode, and designated inductor.

With a duty cycle of $d_1$ for the switch $S_1$ and an $i_2$ current via the MPPT diode $D_3$, the output voltage, $V_2$, of the MPPT subsystem will produce a constant voltage as long as the input parameters stay unchanged. It is the same voltage as the dc LINK voltage. Figure 4 BESS depicts a battery bank (BESS)

with voltage E and internal resistance to aid in energy storage and retrieval in the scenario that WECS-PMSG is unable to provide power to the DC connection and load.

The dc LINK and BESS [18] are linked using a bidirectional dc to dc converter with two switches that operate S3 and S4, and a duty cycle of $d_2$. When there is enough wind power, the battery charges; otherwise, it supplies electricity by draining it in accordance with demand and grid needs. To connect the output of the DC LINK to the load, a buck step-down converter is used.

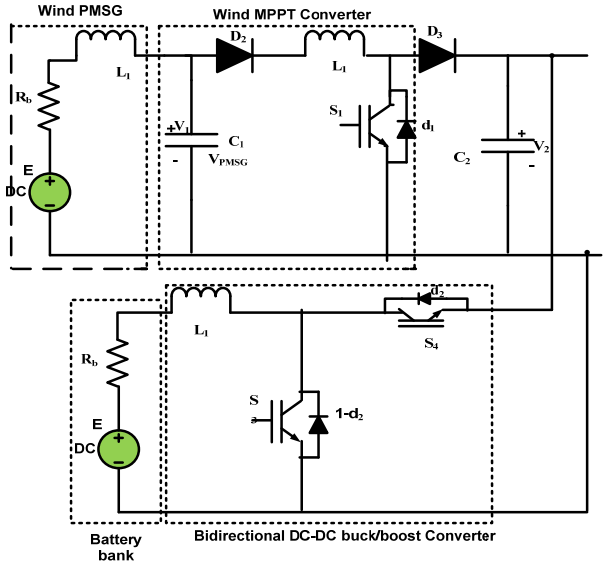


**Figure 4**: Wind PMSG system connected to a DSTATCOM with Battery Energy Storage System

This operation is supported by switch $S_2$ with duty cycle $d_3$, inductor $L_3$, and diode $D_4$. The load converter, which is applied to the load R.L., is the outcome of the dollar voltage across the capacitor $C_2$. The voltage and current formulae are displayed

Equation (1a) provides the changing expression for the input current from the WECS-PMSG.

$$L_1 \frac{di_1}{dt} = V_1 - V_2(1 - d_1) \quad (1a)$$

As demonstrated in equation (1b), Kirchhoff's Current Law (KCL) and Kirchhoff's Voltage Law (KVL) are applied to derive the fluctuating voltage and current equations for each subsystem. Using KCL at the input node, the equation for the input current ($i_1$) from the WECS-PMSG may be obtained. The voltage $V_1$ (WECS-PMSG), the duty cycle $d_1$ of switch S1, and the boost converter's component parameters are probably going to be involved in this equation. The equation corresponding to the battery's dynamic current flow ($i_2$) can be obtained from KCL at the BESS connection node. The battery voltage (E), internal resistance ($R_b$), duty cycle ($d_2$) of switch $S_3$ (bidirectional converter), and other pertinent component values are probably going to be included in this equation.

$$L_2 \frac{di_2}{dt} = E - i_2 R_b - V_2 d_2 \quad (1b)$$

Switch $S_2$ with duty cycle $d_3$ regulates the DC-link voltage ($V_2$), which in turn governs the buck converter. Through the load resistance (RL), the load voltage ($V_3$) generates the load current ($i_3$). Equation (1c) represents the mathematical relationship for $V_3$.

$$L_3 \frac{di_3}{dt} = (V_2 - i_3(1 - d_3)R_L)(1 - d_3) - V_3 \quad (1c)$$

The fluctuating nature of the voltage ($V_1$) across the output capacitor ($C_1$) of the WECS-PMSG cell is described by equation (2a). The difference between the boost converter current ($i_1$) and the source PMSG current ($i_{PMSG}$) produces this voltage. The diode voltage constant, represented by the letter "a," and the diode current ($i_D$) are probably also included in the formula.

$$C_1 \frac{dV_1}{dt} = i_s - i_1 = i_{PMSG} - i_D(e^{aV1} - 1) - \frac{V_1}{R_p} - i_1 \quad (2a)$$

The DC-link voltage's dynamic behaviour is represented by equation (2b). The duty cycles ($d_1$, $d_2$, and $d_3$) of the IGBT switches in the MPPT boost converter, bidirectional DC-DC converter, and buck converter, respectively, are adjusted to manage this voltage.

$$C_2 \frac{dV_2}{dt} = i_1(1 - d_1) + i_2 d_2 - i_3(1 - d_3) - \frac{V_2}{R_1} \quad (2b)$$

The fluctuation of the load voltage ($V_3$) on the DC-link is represented by equation (2c).

$$C_3 \frac{dV_3}{dt} = i_3 - \frac{V_3}{R_2} \quad (2c)$$

The capacitance (C1) of the capacitor regulating the WECS-PMSG's output voltage can be calculated using equation (3). This capacitance value is calculated by scaling down a common base capacitance by a factor of five.

$$C_1 = \frac{0.01}{0.05 C_b} \quad (3)$$

The highest possible ripple current through inductor $L_1$ is given by equation (4a), assuming that the filter capacitor sufficiently suppresses voltage ripple on the DC link, so that the Dc link's power factor variation stays within a 5% tolerance. The converter's switching time constant ($T_{sw}$) and this ripple current are connected.

$$\Delta I_{L1max} = \frac{2V_{dc}}{3L_1}(1 - d_1) d_1 T_{sw} \quad (4a)$$

Instead of using the switching time constant ($T_{sw}$), equation (4b) expresses the maximum ripple current for inductor $L_1$ in terms of the switching frequency ($F_{sw}$). This formula most likely takes the IGBT switch's duty cycle (d1) of 0.5 into account ($S_1$).

$$\Delta I_{L1max} = \frac{V_{dc}}{6 F_{sw} L_1} \quad (4b)$$

To find the maximum ripple from the panel MPPT output, use equation (4c) to calculate the maximum allowable ripple current in the MPPT output based on a 10% ripple tolerance of the rated current.

$$\Delta I_{L1max} = 0.1 \Delta I_{max} \quad (4c)$$

The link between the WECS-PMSG panel's maximum output current and two important variables the WECS-PMSG real power ($P_{PMSG}$) and the WECS-PMSG input voltage ($V_{PMSG}$), which is also referred to as V1 in earlier equations is expressed in equation (5).

$$I_{max} = \frac{\sqrt{2} P_{PMSG}}{V_{PMSG}} \quad (5)$$

A method for determining the inductances (L1 and $L_2$) needed for the battery-DC link bidirectional converter inductor and the MPPT boost converter inductor is provided by equations (6a) and (6b), respectively. The attenuation factor Ka is most likely responsible for the 20% current ripple reduction that these calculations seek to achieve.

$$L_1 = \frac{V_{dc}}{6 F_{sw} \Delta I_{L1max}} \quad (6a)$$

$$L_2 = \frac{1+\frac{1}{\sqrt{K_a^2}}}{C_2\omega_{sw}^2} \quad (6b)$$

The system's potential for resonant situations is lessened by resistors R1 and R2. They also help to lessen the ripple in switching frequencies. The value of resistor R1 is probably expressed by equation (7a) depending on the angular resonance frequency ($\omega_{res}$, rad/sec).

$$R_1 = \frac{1}{3C_2\omega_{res}} \quad (7a)$$

where the Equation (7b) defines the angular resonance frequency ($\omega_{res}$, rad/sec).

$$\omega_{res} = \sqrt{\frac{L_1+L_2}{L_1L_2C_2}} \quad (7b)$$

The final DC-link voltage is expressed in equation (8) as a function of all the subsystem voltages taken into account in the model. This implies a vectorial summation method in which the total DC-link voltage is represented by mathematically summing the individual subsystem voltages.

$$V_2 = V_{20} + \frac{1}{C_2}\int_0^T (I_{PMSG,out} + I_{BESS} + I_{grid,out} - I_{charging})dt \quad (8)$$

For the WECS-PMSG MPPT subsystem, the initial bus voltage is $V_{20}$.Value of the DC microgrid (MG) capacitor is $C_2$. At time t, the WECS-PMSG panel MPPT subsystem's output current is represented by IPMSG, out(t). Positive charging current and negative discharging current make up the IBESS (also known as $I_2$). $I_{grid,\ out}$. The total current output of the grid. In equation (9a), the BESS charging current is expressed

$$I_{charging} = \frac{P_{charging}}{V_2\eta_{DC-DC1}} \quad (9a)$$

Equation (9a) likely relates the BESS charging current to the real power flowing through the charging terminal. This real power flow depends on the inductance ($L_1$) and the DC-DC bidirectional converter's efficiency ($\eta_{DC\text{-}DC1}$). It's important to note that this efficiency might also be influenced by the load chopper converter's operation. Equation (9b) likely defines the DC-link current output ($I_{grid}$, out) based on the DC-link real power ($P_{grid}$), DC-link voltage ($V_2$), and the grid boost voltage conversion efficiency (ηDC-DC2).

$$I_{grd,out} = \frac{P_{grid}}{V_2}\eta_{DC-DC2} \quad (9b)$$

Equation (9c) likely expresses the BESS current flowing into the DC microgrid (MG) as a function of the battery voltage (E), the battery cell current (IBESS), and the bidirectional DC-DC converter's efficiency (ηDC-DC3).

$$I_{BESS,out} = \frac{EI_{BESS}}{V_2}\eta_{DC-DC3} \quad (9c)$$

Equation (10) defines the load voltage ($V_{load}$ or $V_3$) as a function of the buck converter's switching duty cycle ($d_3$).

$$V_{load} = V_2\frac{1}{1-d3} \quad (10).$$

Equation (11a) describes the relationship between the dynamic DC-link current (i_mg) and the DC-link voltage (Vdc). This relationship involves the current through diode $D_2$ and the switching duty cycle ($d_2$) of the bidirectional buck-boost converter. The constant term 'a' likely controls the converter's operation mode: a value of 1 corresponds to boost operation, while -1 corresponds to buck operation. Therefore, the duty cycle ($d_2$) plays a crucial role in controlling the buck or boost operation of the converter, ultimately influencing the grid currents.

$$\frac{dV_{dc}}{dt} = a(-\frac{i_{mg}}{C_2} + \frac{d_2i_2}{C_2}) \quad (11a)$$

The dynamic behavior of the current ($i_{L2}$) flowing through the inductor (L2) of the bidirectional buck-boost converter represented in Equation (11b). This equation likely considers both the battery voltage (E) and the DC microgrid (MG) voltage ($V_2$).

$$\frac{di_{L2}}{dt} = a(\frac{E}{L_2} - d_2\frac{V_2}{L_2}) \quad (11b)$$

The transfer function relating the dynamic current ($i_{L2}$) of the bidirectional buck-boost converter inductor (L2) to the DC microgrid (MG) capacitor ($C_2$) expressed as in Equation (11c). This transfer function is likely represented in the Laplace domain using the Laplace variable 's'.

$$\frac{\bar{i}_{L2}}{\bar{d}_2} = \frac{-C_2V_2s - d_2i_{L2}}{C_2L_2s^2 + d_2^2} \quad (11c)$$

Equation (12a) describes the construction of a current-controlled PI controller for controlling the DC-link voltage ($V_2$). This controller takes two inputs: the reference current of the inductor boost converter subsystem and the actual boost converter current. The proportional and integral gains $K_{pi}$ and $K_{ii}$ PI controllers are designed to minimize the error between these two currents. As a result, this helps to manage the voltage across the DC link.

$$\bar{V}_2 = (\bar{i}_{L1}^* - \bar{i}_{L1})(K_{pi} + \frac{1}{K_{ii}s}) \quad (12a)$$

Equation (12b) represents the final terminal voltage ($V_2$) of the DC-link transfer function in relation to the input current ($i_{L1}$) from the WECS-PMSG. This transfer function takes into account the boost converter duty cycle ($d_1$) and the current-tuned proportional-integral (PI) controller.

$$\frac{\bar{V}_2}{\bar{i}_{L1}^*} = \frac{-K_{pi}K_{ii}d_1V_2s - d_1V_2}{C_2s^3 - C_2V_2K_{pi}K_{ii}s^2 + (d_1^2K_{ii} - C_2V_2)s} \quad (12b)$$

### 3.2 Block diagram representation of WECS-PMSG system

Figure 5 depicts the DC link with a closed-loop control system for the WECS-PMSG cell, as discussed in Section 2. The block diagram contains a $G_{PI}(s)$, which depicts a current-tuned proportional-integral (PI) controller. ($G_{sw}(s)$) is the offset switching frequency block (function unclear without context), $G_{PMSG}(s)$ is the transfer function representing the WECS-PMSG panel system connected to the DC link, and $A_v(s)$ is the DC voltage gain function defined by us. Equation (13a) uses the Laplace variables to define the current PI controller. The controller has two parameters: the current integral constant ($K_{ii}$) and the current proportionality constant ($K_{pi}$).

$$G_{PI}(s) = K_{pi} + \frac{K_{ii}}{s} \quad (13a)$$

Equation (13b) describes the offset switching block's ($G_{SW}(s)$) function. In that it modifies its operation in response to variations between the reference dc-link voltage ($V^*_2$) and the actual dc-link voltage ($V_2$), this block functions similarly to a relay.

$$G_{SW}(s) = \begin{cases} 1 & V_2 > V_2^* \\ 0 & V_2 < V_2^* \end{cases} \quad (13b)$$

Equation (13c), which represents the transfer function ($G_{PMSG}(s)$) of the WECS-PMSG panel system as a typical second-order function, has the natural undammed frequency ( $\omega_n$ ) and the damping ratio as ( $\xi$ ).

$$G_{PMSG}(s) = \frac{\omega_n^2}{s^2+2\xi\omega_n s+\omega_n^2} \quad (13c)$$

A number of variables, including the switching duty cycle ($d_2$) of the BESS converter, the inductance ($L_1$) of the WECS-PMSG panel inductor, and the DC-link voltage across the capacitor ($C_2$), may have an impact on the DC-DC link voltage gain.

$$A_v(s) = \frac{1-d_2}{L_1C_2s^2+\frac{L_1}{R_1}s+(1-d_2)^2} \quad (14)$$

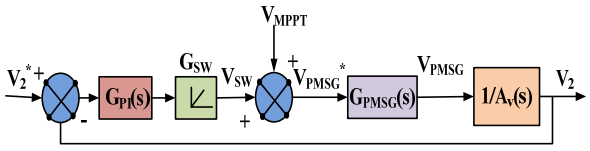


**Figure 5.** Wind PMSG connected to a DSTATCOM block diagram representation

The transfer function in Equation (15a) relates the DC-link terminal voltage ($V_2$) to multiple factors influencing the Maximum Power Point Tracking (MPPT) system. These factors include the DC link's initial voltage ($V_{20}$), the source's MPPT voltage ($V_{mppt}$), which is taken to be constant in this work, the transfer function that represents MPPT output limitations ($G_{olimit}(s)$), and the transfer function of the MPPT control system ($G_{omppt}$).

$$V_2 = G_{olimit}(s)V_{20} - G_{omppt}V_{mppt} \quad (15a)$$

The internal transfer functions employed in equation (15a) are probably defined by equations (15b) through (15d). A more thorough explanation of the variables affecting the DC-link terminal voltage ($V_2$) in the MPPT system may be found in these internal functions.

$$G_{olimit}(s) = \frac{G_{PI}(s)G_{SW}(s)G_{PMSG}(s)}{G_{PI}(s)G_{SW}(s)G_{PMSG}(s)-A_V(s)} \quad (15b)$$

$$G_{omppt}(s) = \frac{G_{SW}(s)}{G_{PI}(s)G_{SW}(s)G_{PMSG}(s)-A_V(s)} \quad (15c)$$

$$G_{vmppt}(s) = \frac{\Delta V_2}{\Delta V_{mppt}} = -\frac{G_{PI}(s)}{G_{PI}(s)G_{PMSG}(s)-A_V(s)} \quad (15d)$$

The error signal in the DC-link voltage control system is represented by equation (16).

$$\Delta V_2 = V_2^* - V_2 = \lim_{s\to 0} s\Delta V_2 = 0 \quad (16)$$

Equation (17) expresses the transfer function ($G_{ov}(s)$) that represents the final voltage of the dc link voltage terminal. This transfer function most likely connects the output voltage to the controller's transfer function ($G_{ov}(s)$). Equation 13c defines the transfer function of the WECS-PMSG panel system, and the voltage gain of the DC-DC converter is impacted by the previously described parameters.

$$G_{ov}(s) = G_{PI}(s)G_{PMSG}(s)\frac{1}{A_V(s)} \quad (17)$$

### 3.3 Structure of Proposed DSTATCOM WECS PMSG MPPT using FLC control

This section describes the enhanced fuzzy logic controller (FLC) design and parameter tuning used in the WECS PMSG MPPT system. The signal duty cycle (D), which controls the power converter switching in the WECS system and eventually influences the power output, is the FLC's output. Changes in error (ΔE) over time are regarded as inputs, as they help maintain the difference between the desired maximum power point (MPP) and the actual operating point [15]. For simplicity, triangular membership functions are employed.

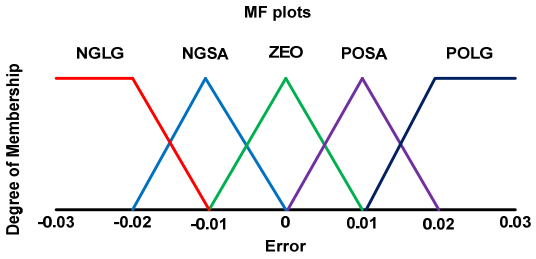


**Figure 6(a):** Error's Membership Functions (MFs) in MPPT Control

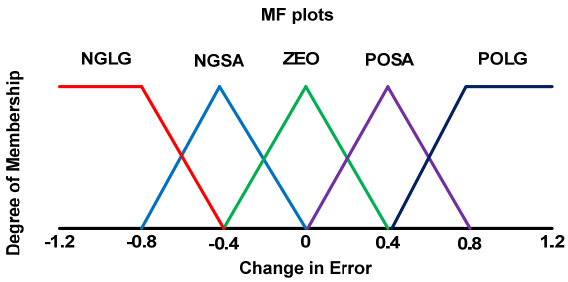


**Figure 6(b):** Membership Functions (MFs) of Change in Error for MPPT Control

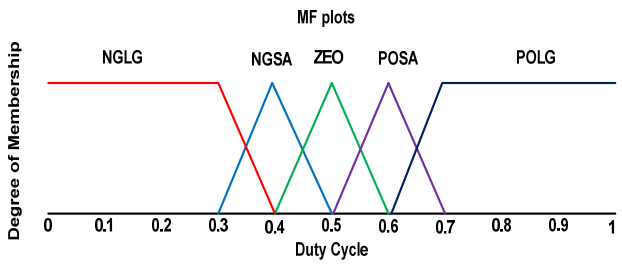


**Figure 6(c):** Membership Functions (MFs) of Duty Cycle for MPPT Control

**Table 1:** Fuzzy Rule Base for MPPT Control

| *E* | *CE* | | | | |
|---|---|---|---|---|---|
| | **NGLG** | **NGSA** | **ZEO** | **POSA** | **POLG** |
| **NGLG** | ZEO | ZEO | POL | POLG | POLG |
| **NGSA** | ZEO | ZEO | POS | POSA | POSA |
| **ZEO** | POSA | ZEO | ZO | ZEO | NGSA |
| **POSA** | NGSA | NGSA | NGS | ZEO | ZEO |
| **POLG** | NGSA | NGLG | NGL | ZEO | ZEO |

**Table 2:** Fuzzy Rule Base

| E | CE | | | | |
|---|---|---|---|---|---|
| | **NGLG** | **NGSA** | **ZEO** | **POSA** | **POLG** |
| **NGLG** | ZEO | ZEO | POLG | POLG | POLG |
| **NGSG** | ZEO | ZEO | POSA | POSA | POSA |
| **ZEO** | POSA | ZEO | ZEO | ZEO | NGSA |
| **POSA** | NGSA | NGSA | NGSA | ZEO | ZEO |
| **POLG** | NGSA | NGLG | NGLG | ZEO | ZEO |

As shown in Figure, these functions specify each input and output value's degree of inclusion within fuzzy sets. The MF is adopted in 6(a), 6(b), and 6(c). For the fuzzy logic controller's (FLC) inputs and outputs, five fuzzy sets are used. These sets are referred to as Negative Large (NGLG), Negative Small (NGSA), Zero (ZEO), Positive Small (POSA), and Positive Large (POLG). The input and output membership functions are displayed in Figure 6. Tables 1 and 2 demonstrate the fuzzy rule foundation that is used for Maximum Power Point Tracking (MPPT). It's vital to remember that the FLC can replace the PI controller in a DSTATCOM controller, and the same explanation can be applied to it.

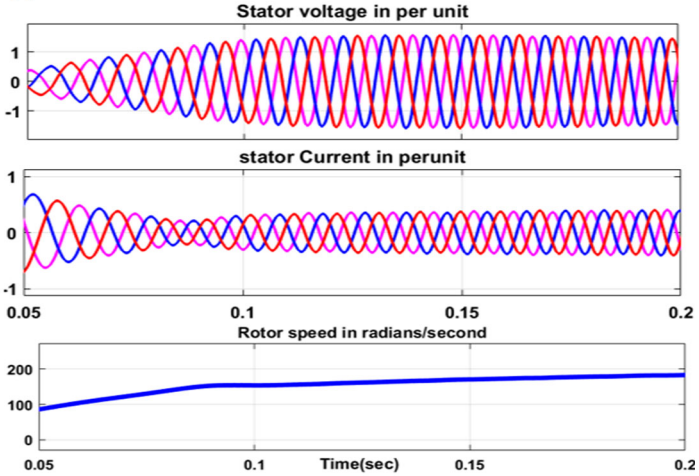


**Figure 6(d):** Simulation results of the WECS.

Figure 6(d) represents the simulation results of WECS with PI control, showing stator voltage and current in per unit, and rotor speed in radians/second, highlighting system performance. The results emphasize the effectiveness of the combined Fuzzy MPPT and PI control in regulating voltage, current, and rotor speed, contributing to enhanced power quality and system stability.

### 3.3.1 Advantages of FLC-based MPPT in WECS

- **Dynamic Response**: Due to FLC's rule-based methodology, which enables quick adaptation to variations in wind speed and smoothest out control operations, less oscillation occurs near the maximum power point (MPP), reducing mechanical stress on the wind turbine, and faster convergence to the MPP is possible.
- **Complex Decision-Making**: By processing several inputs at once, including power output, rotor speed, and wind speed, FLC is able to make more intelligent and effective control decisions. It can improve the control strategy's efficacy under a range of operating settings by using expert insights and heuristic knowledge.
- **Implementation Flexibility**: It is simple to scale and adapt FLC-based MPPT to various wind turbine and generator types. Since they rely on qualitative descriptions rather than exact mathematical definitions, these are simpler to tune than PID controllers.
- **Adaptability and Robustness**: Wind turbines and generators have nonlinear features that can be efficiently handled by FLC-based MPPT. In contrast to conventional MPPT techniques, which frequently depend on linear models, FLC is resilient to changes in parameters and outside disruptions and adjusts to the nonlinear and unpredictable nature of wind energy. It can continue to function in the face of abrupt changes in wind conditions and a range of wind speeds.
- **No Need for Precise Mathematical Model**: FLC is less dependent on exact system parameters and is easier to implement because it does not require a perfect mathematical model of the system. In wind energy systems, where it might be difficult to obtain an accurate model, this is very helpful.

### 3.4 DSTATCOM with WECS-PMSG Controlled using ANN-PI Controller

The application of an ANN-PI controller for a DSTATCOM in a PMSG-based Wind Energy Conversion System (WECS) will be addressed in this section. The fundamental job of the DSTATCOM, not the PMSG, is to reduce supply harmonic currents while maintaining a steady DC-link voltage. Figure 7 depicts the shunt VSC and proposed controller. Three layers structure an ANN: an input layer, an output layer, and a hidden layer with 100 neurons. The error signal, which is the distinction between the reference DC-Link voltage ($V_{refdc}$) and the actual DC-Link voltage, is received by the input layer. The input layer of the ANN receives real-time data, including load currents ($i_{lab}$, $i_{lbc}$, and $i_{lac}$) and the DC-link loss component ($\Delta i_{dc}$). These reference currents most likely serve to regulate power flow and manage converter switching. Figures 7(a) through 7(f) probably show how the back-propagation neural network design is used in the ANN controller. Given that 200 hidden layer neurons are mentioned, a reasonably intricate network architecture is implied. The output of the trained ANN is reference currents. These reference currents are then used by a hysteresis current controller with adjustable bands (e.g., ±0.25 A or ±0.5 A) to generate switching pulses (Sa1, Sa2, Sb1a, Sb2, Sc1, Sc2) for the shunt converter. An input layer (IL), a hidden layer (HL), and an output layer make up an ANN (OL). The input layer passes the load currents and DC-link loss it receives to the hidden layer after storing it. The input data is multiplied by the

matching weights connected to the connections between neurons in the preceding layer and the current hidden layer within the hidden layer. In essence, these weights indicate how strong these linkages are. After adding up all of the weighted data points, a hidden layer bias and a non-linear activation

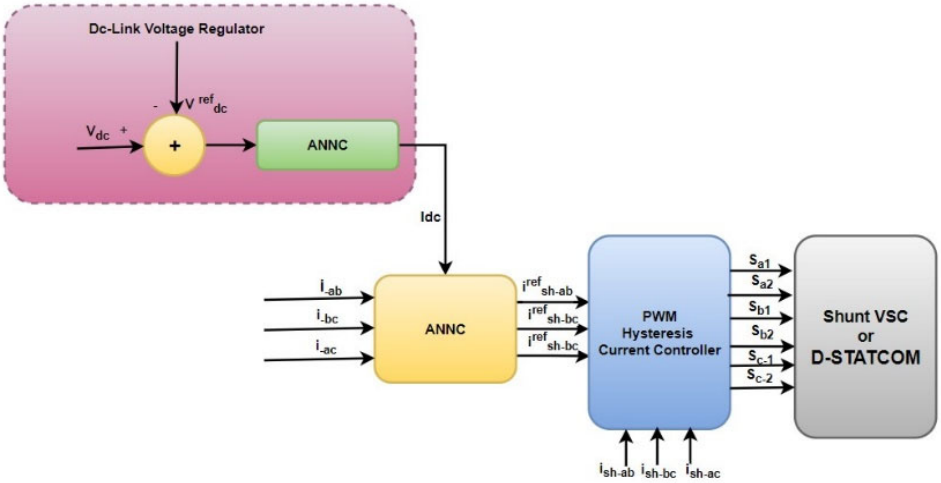


**Figure 7(a):** DSTATCOM as a Shunt VSC Controller for power quality enhancement with ANN-PI controller (ANNC)

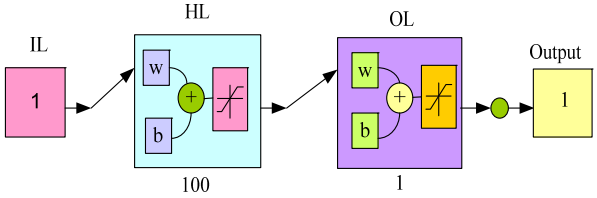


**Figure 7(b):** Schematic of Multi-Layer Perceptron for DC-Link Voltage Balancing

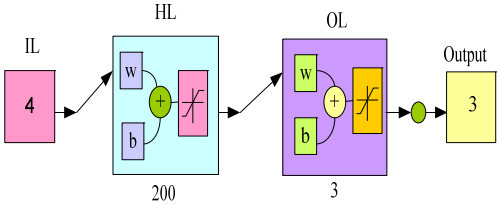


**Figure 7(c):** Block Diagram of ANN for Reference Current Generation.

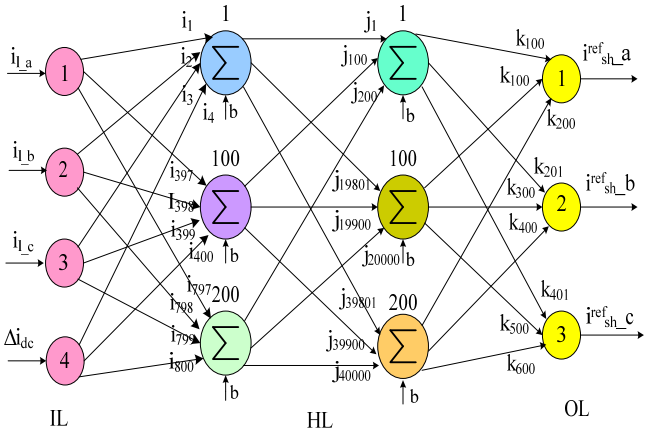


**Figure 7(d):** Detailed Schematic of Multi-Layer Perceptron with Backpropagation for Reference Currents

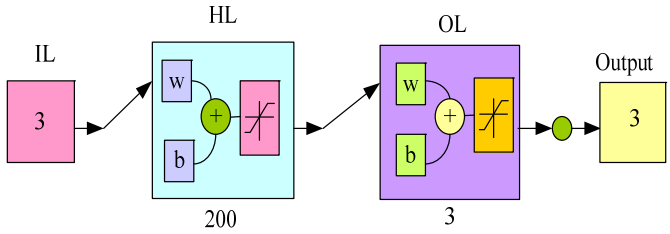


**Figure 7(e):** ANN structure for reference voltage generation.

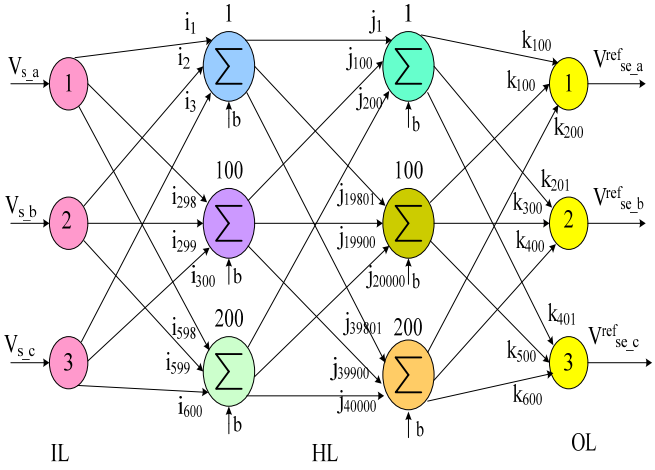


**Figure 7(f):** DSTATCOM DC-Link Regulation:

Backpropagation ANN Architecture for reference voltage predictionfunction which isn't stated directly in this context—are applied. This activation function gives the network non-linearity, allowing it to simulate complex interactions between the input and output. The activation values of the neurons in the buried layer subsequently store the outcomes of these computations.

A feed-forward error back-propagation architecture is used in this implementation. Iterative adjustments are made to the weights during the training period. For a particular set of input data (load currents and DC-link voltage loss), the network computes the error between its output (predicted reference currents) and the target data (desired reference currents). In order to attain faster convergence than ordinary

backpropagation, the Levenberg-Marquardt backpropagation (LMBP) training algorithm is utilized. The ANN controller learns to map the input data to the proper reference currents for the shunt converter by iteratively fine-tuning the weights based on the computed error, guaranteeing efficient DSTATCOM operation.

### 3.5 Battery storage system

The BESS controller circuit, which includes a bi-directional buck-boost converter, is shown in Figure 8. This converter, which is probably managed by a PIC microprocessor, is essential to keeping the DC bus voltage steady. It is likely that equation (23) describes the battery's state-of-charge (SOC).

$$SOC = 100(1 + \int i_{BSS}\ dtQ) \quad (18)$$

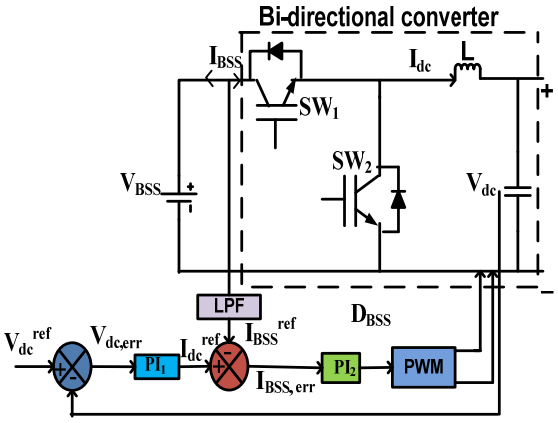


**Figure 8:** Block Diagram for the Bi-Directional Buck-Boost Converter used in BESS Integration

The BESS operation mode (charging or discharging) is determined by two factors: the battery's state-of-charge (SOC) limits defined in Eq. (24) and the available power generation from the solar system.

$$SOC_{\min} \le SOC \le SOC_{\max} \quad (19)$$

Where,

$Q$=Battery capacity.

$V_{BSS}$ = Voltage across the battery terminals.

$i_{BSS}$= Current passing from or the battery.

The reference current for the battery ($i^{ref}{}_{dc}$) is determined by minimizing the DC-link voltage error ($V_{dc,err}$). Equations (4) and (5) likely describe this minimization process, which is implemented using a PIC controller. The PI controller then regulates the battery current error ($i_{BSS,err}{}^{*}$) to achieve the desired reference current. The battery current error is the difference between the reference DC-link current ($i^{ref}{}_{dc}$) and the actual battery current ($i^{ref}{}_{BSS}$) obtained from a low-pass filter (LPF). Equations (26) to (28) likely define the implementation of this PI control strategy.

$$V_{dc,err}(t) = V^{ref}{}_{dc} - V_{dc} \quad (20)$$

$$i^{ref}{}_{dc} = K_{p,1}\ V_{dc,err}(t) + K_{i,1} \int_0^t V_{dc,err}(t)\ dt \quad (21)$$

$$i_{BSS,err}(t) = i^{ref}{}_{dc} - i^{ref}{}_{BSS} \quad (22)$$

$$i_{BSS,err}{}^{*} = K_{p,2}\ i_{BSS,err}(t) + K_{i,2} \int_0^t i_{BSS,err}(t)\ dt \quad (23)$$

Where,

$$i^{ref}{}_{BSS} = \left(\frac{1}{1+T.S}\right) * i_{BSS} \quad (24)$$

$PI_1$and $PI_2$controller gains are heuristically chosen as $K_{p1}$=1.5, $K_{i1}$=0.1, $K_{p2}$=1.477 and $K_{i2}$=3.077. Table explains the power distribution at DC-Link of the proposed DSTATCOM-PMSG-WECS-BESS.

### 3.6 The Fuzzy granular Technique for Power Quaity improvement using DSTATCOM-PMSG-WECS

The two main problems with fuzzy control systems used in industry are rule explosion and complex structure [14]. The fuzzy controller design process is the first step in this paper's fuzzy control technique, which is based on granular computing. Each fuzzy rule is then given the information granulation technique, which turns it into an information granule. In place of the fuzzy controller, granule points are used to fit the granular function's realization function, which is then used to control the item. If control precision is maintained, rule explosion can be effectively avoided in the fuzzy control system based on granular computing, where the number of rules is simply related to the number of granules. Simultaneous removal of fuzzy reasoning, defuzzification, and fuzzification lowers processing complexity and simplifies the structure of systems.

The application of the fuzzy granular approach in Simulink is shown in Figure 9. Due to non-linear loads, the fuzzy-granular method is now being employed to improve the power quality of the source side current waveform. The fuzzy-granular control system receives the error or controller parameter as input. Here, linear regression techniques are used to transform non-linear parameters into linear parameters. Regression analysis also makes use of sliding mode control.

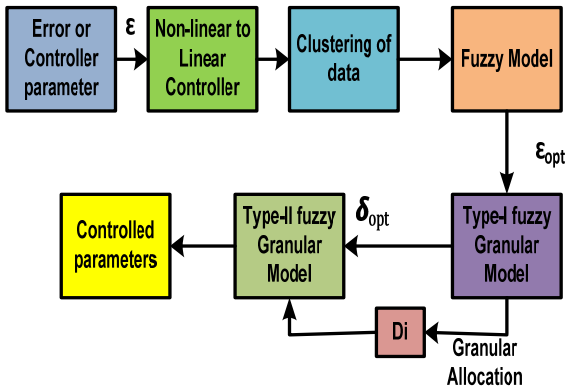


**Figure 9:** Fuzzy-Granular Controller for DSTATCOM-PMSG-WECS

The linear models are given into the fuzzy model as clusters or granules. Before being submitted to the Type-I fuzzy-granular model for error optimization, the error is now minimized. The Type-II fuzzy controller receives these values after the data has been transformed into optimal parameters using a granular allocation block, allowing for efficient control of the error parameter. To obtain the regulated parameter, the gain settings of this Type-II fuzzy controller are modified. The

dc link voltage error is one of the error controller parameters in this case. It is fed into the fuzzy-granular controller model and processed with the current parameter being the final output.

## 4. RESULT ANALYSIS

### 4.1 PI controller for DSTATCOM-PMSG-WECS under non-linear loads

Figure 10 shows a DSTATCOM-PMSG-WECS that uses a PI controller to correct for power quality issues caused by non-linear loads. The DSTATCOM is operated by a manually adjusted Proportional-Integral (PI) controller. Power quality issues result from these loads distorting the source's current waveform. Figure 10 displays the waveforms; to control the source voltage and enhance its quality, the DSTATCOM injects current and voltages. In Figure 10, the source voltage and current are displayed.

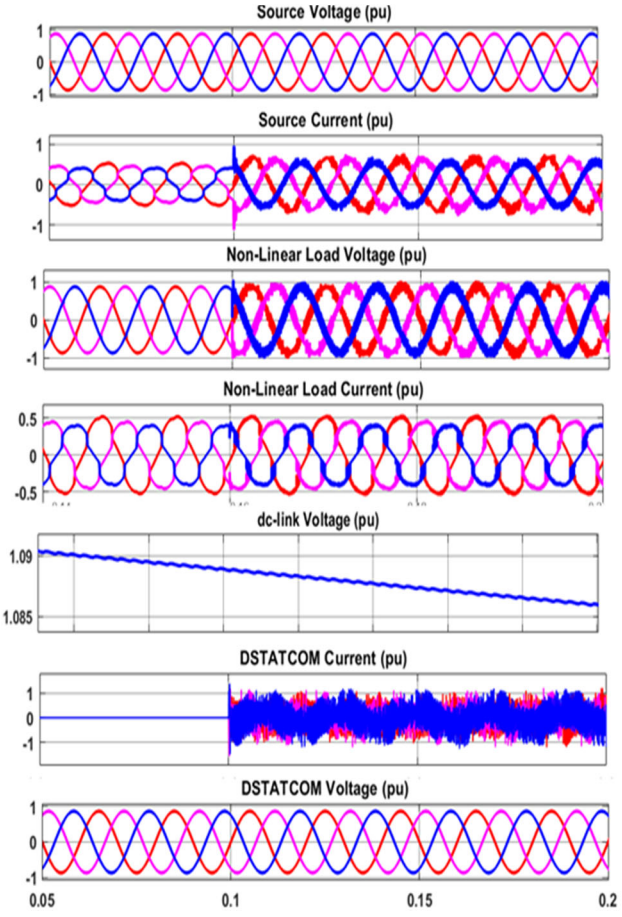


**Figure 10:** System waveforms with PI Controller

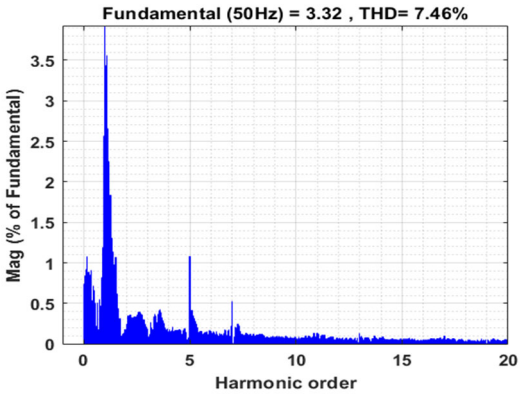


(a)

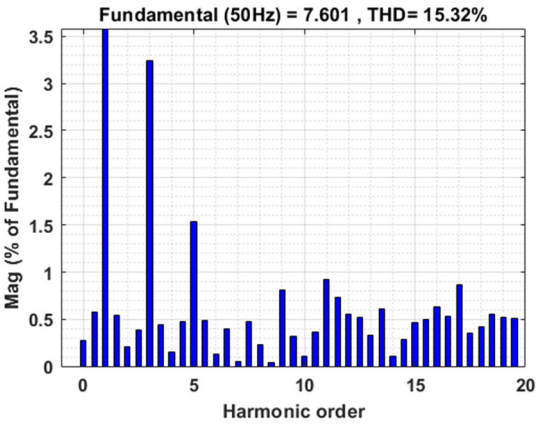


**(b)**

**Figure 11:** (a) Source current THD without controller (b)Load current without controller

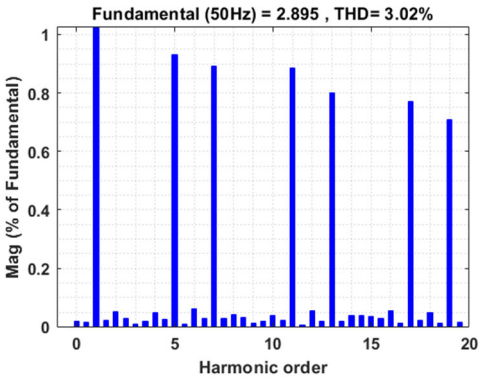


(a)

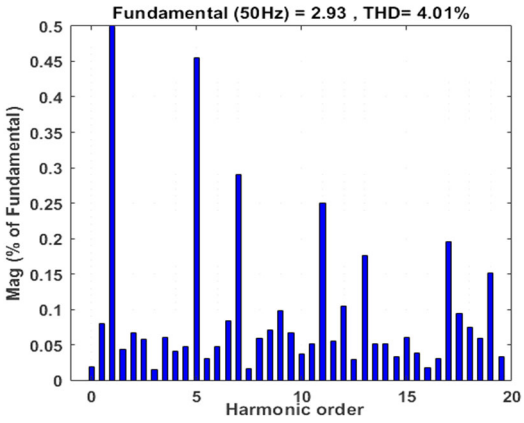


(b)

**Figure 12:** (a) Source current THD PI controller (b)Load current PI controller

As shown in Figures, the Total Harmonic Distortion (THD) source and load currents are 7.46% and 15.32%, respectively Without controllers, 11(a) and 11(b). The Total Harmonic Distortion (THD) source and load currents are 3.02% and 4.01%, respectively, as shown in the figures 12(a) and 12(b) with the PI controller indicating that some harmonic distortion remains. The voltage and current waveforms will be altered as a result of the non-linearity of the load. When the DSTATCOM switch is turned on, the voltage and current drop sharply before returning to and maintaining a steady level.

### 4.2 Performance Analysis of DSTATCOM-PMSG-WECS with Advanced Controllers (ANN-PI and Fuzzy granular controller) under Non-Linear Loads

As seen in Figures 13 and 14, this analysis contrasts the effectiveness of two advanced control strategies for a DSTATCOM-PMSG Wind Energy Conversion System (WECS) under non-linear load situations. Comparing these controllers to the traditional PI controller, there are noticeable benefits. This method, which is an improved version of the fuzzy controller shown in (Figure 14), combines sliding mode control for robust performance during transient events with fuzzy logic for rule-based decision making. In order to learn the intricate link between system inputs (such as source voltage and load current) and the intended control outputs for the PI controller, this method makes use of an Artificial Neural Network (ANN).

Figures 13 and 14 show different waveforms for every controller, giving information about how effective they are. In comparison to the PI controller, the source voltage waveform is improved by all advanced controllers (Figure 10). Different controllers may experience different levels of improvement. Source current harmonics are probably going to be lower with all advanced controllers than with the PI controller, much like with voltage. The controller determines how much of an improvement this is. In comparison to the PI controller, there should be some improvement in the voltage waveforms at the non-linear load terminals in terms of less distortion. In comparison to the PI scenario, the advanced controllers are predicted to produce current waveforms drawn by the non-linear load that are more sinusoidal in shape.

When using a PI controller (Figure 10), the DC-link voltage most likely varies greatly. A lower variance in DC-link voltage is seen with ANN-PI (Figure 13) than with PI. On the other hand, the DC-link voltage exhibits negligible fluctuations when using Fuzzy granular (Figure 14), suggesting that all of the approaches presented have good regulation. The controller technique will determine the differences in the injected voltage waveforms from the DSTATCOM. It's possible that Fuzzy granular will show the best injection for the best possible power quality increase. The DSTATCOM's injected voltage waveforms and current will change depending on the controller. For efficient power quality correction, the most ideal injection profile will probably be obtained using the Fuzzy granular approach.

When compared to a PI controller, the ANN-PI controller performs better in terms of decreased voltage and current harmonics, enhanced DC-link voltage management, and efficient DSTATCOM operation. With near-sinusoidal voltage and current waveforms, the tightest DC-link voltage control, and possibly the best DSTATCOM injected voltage and current profiles for improving power quality, the Fuzzy granular exhibits the most improvement. When applied to non-linear load situations, the advanced control approaches (ANN-PI, Fuzzy granular) greatly enhance the DSTATCOM-PMSG-WECS's performance in comparison to the traditional PI controller. The most efficient controller between the two is fuzzy granular, which provides improved DC-link voltage regulation, better power quality improvement, and maybe better DSTATCOM functioning

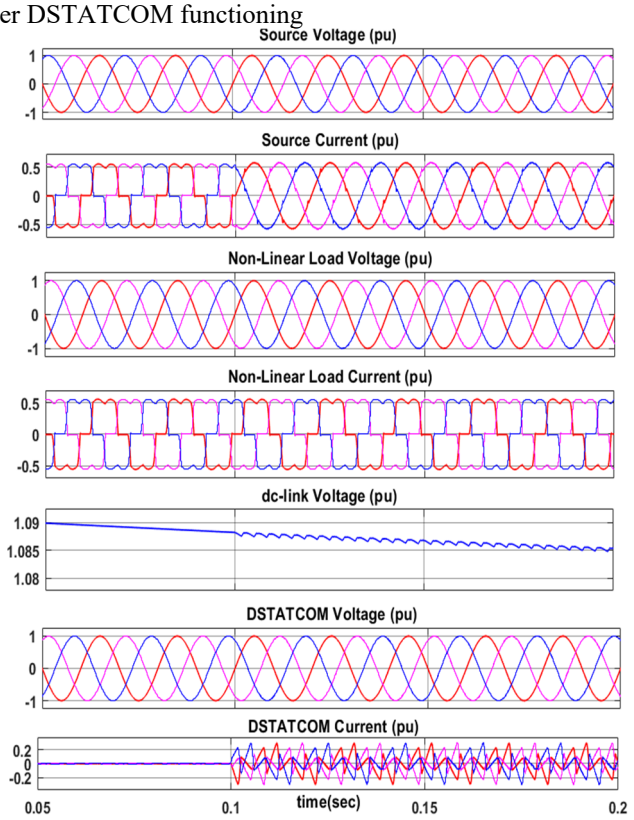


**Figure 13:**System wave form with ANN-PI

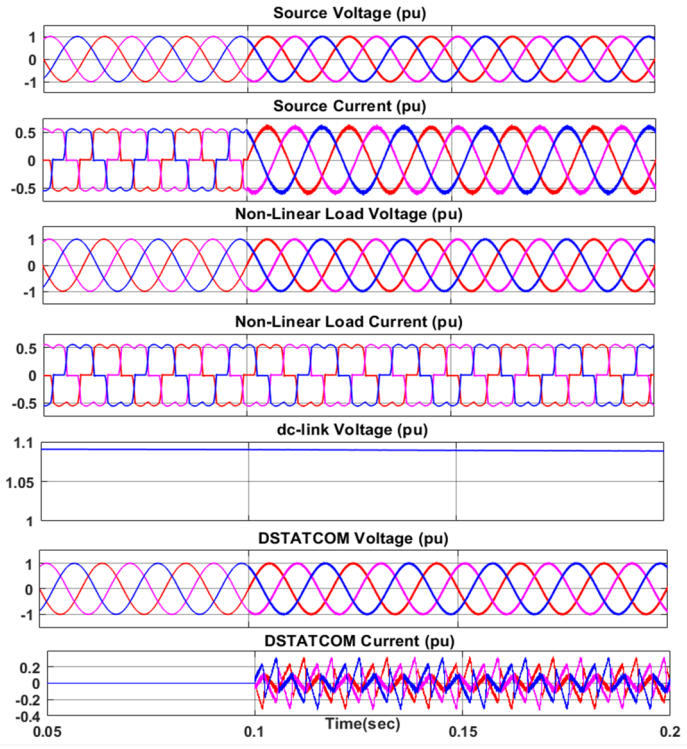


**Figure 14:** System waveforms with Fuzzy-Granular

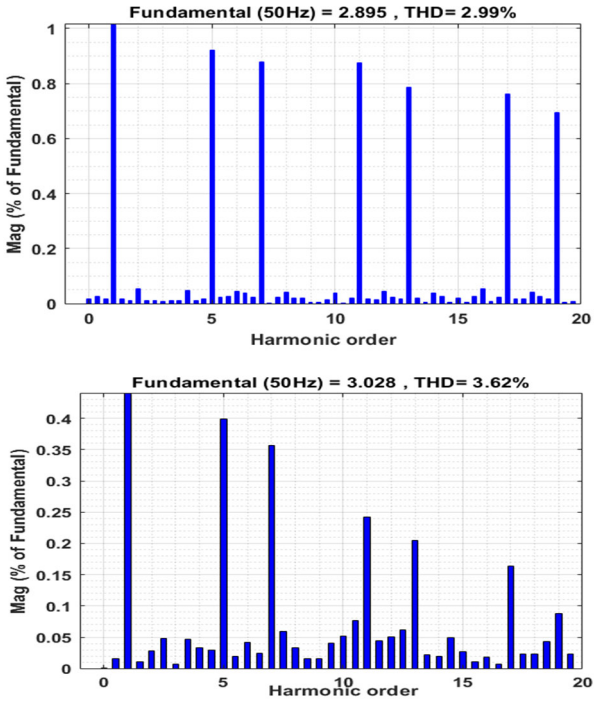


(b)

**Figure 15:** (a)THD of the source current using an ANN-PI controller (b)THD of the load current using an ANN-PI controller

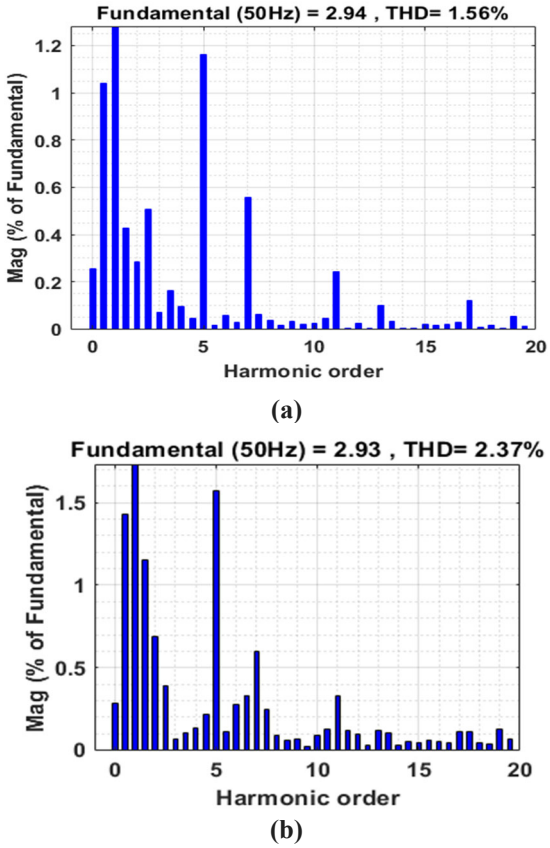


**Figure 16:** (a)THD of the source current using Fuzzy granular-PI (b) THD of the Load Current with Fuzzy granular

The source-side Total Harmonic Distortion (THD) of the source current utilizing different control techniques is displayed in Figures 15(a) and 16(a) for a DSTATCOM-PMSG Wind Energy Conversion System (WECS) operating under non-linear load conditions. The examination contrasts two controllers' performances. As illustrated in Figure 15(a), the source current THD of the ANN-PI control is 2.99%, while Figure 16(a) displays the Fuzzy granular control's THD of 1.56%. All of the controllers are seen to dramatically lower the source current's THD in order to mitigate current harmonics. The power quality of the DSTATCOM-PMSG-WECS system is greatly impacted by the controller selection, as may be concluded from this result analysis. The THD research reveals that the best controllers for lowering current harmonics and enhancing overall power quality are ANN-PI and Fuzzy granular.

Figures 15(b) and 16(b) show the way advanced control techniques enable a significant reduction in load current Total Harmonic Distortion (THD) for a DSTATCOM-PMSG Wind Energy Conversion System (WECS) under non-linear load situations. The results from the earlier figures (Figure 14, Figure 15) are expanded upon in this examination. The high THD (4.01%) of the load current with a traditional PI controller is probably shown in Figure 12(b). The efficacy of Fuzzy Granular and ANN-PI advanced controllers in reducing source current harmonics was illustrated in Figures 15 and 16. When compared to the PI controller, ANN-PI (Fig. 15(a)) obtains a THD of 3.62%, which is a significant reduction. With a very low THD of 2.37%, the Fuzzy granular shows the biggest improvement, demonstrating its remarkable harmonic mitigation capacity. When compared to the PI controller, the load current THD is greatly decreased by the advanced controllers (ANN-PI, Fuzzy Granular). Fuzzy granular outperforms conventional controllers by attaining the lowest THD, demonstrating its exceptional efficacy in guaranteeing load currents that are almost sinusoidal. With advanced controllers, load current THD is dramatically reduced, which improves system power quality. By doing this, possible power losses are minimized, equipment stress is decreased, and grid stability is improved. These controllers provide improved power quality for the DSTATCOM-PMSG system and the linked loads by efficiently reducing harmonics.

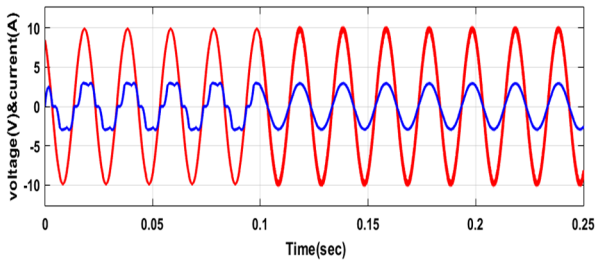


**Figure 17:** The source voltage and current are both in phase with Fuzzy granular controller

The connection between the wind turbine and nonlinear load affects the source voltage and current. Consequently, both the source side and the PCC have an impact on the wave shape. At t = 0.1s, the grid and the DSTATCOM are connected. In this case at PCC, Figure 17 source voltage and current waveforms demonstrate how the reactive demand and system harmonics begin to drop after 0.1 seconds of DSTATCOM operation. In addition, the source voltage and current of PCC are in phase, suggesting that the power factor is kept close to unity. The DSTATCOM minimizes source voltage harmonics in addition to source current.

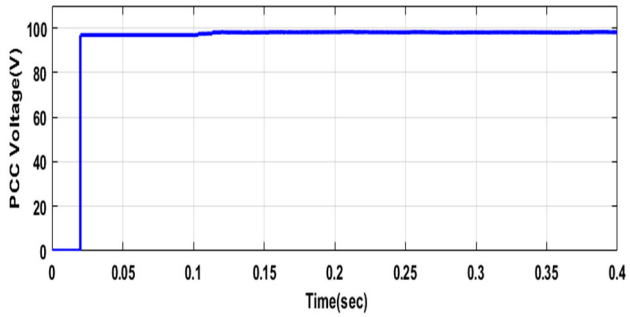


**Figure 18:** Voltage magnitude at PCC with Fuzzy granular controller

At PCC, the voltage magnitude remains at 100V following the connecting of DSTATCOM. The voltage's harmonics are eliminated at PCC. Figure 18 displays the voltage magnitude. Reactive power adjustment using a fuzzy granular approach with a DSTATCOM is shown in Figure 19 for a system with nonlinear loads. This efficient adjustment demonstrates how the DSTATCOM's fuzzy granular approach can preserve power quality and regulate reactive power even when nonlinear loads are present.

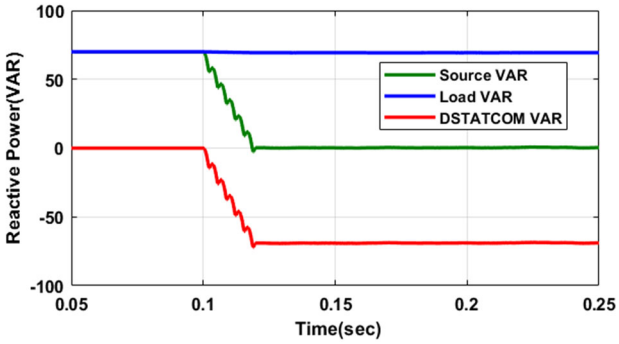


**Figure 19:** Reactive Power Compensation with Fuzzy granular controller

Proportional (Kp) and integral (Ki) gains must be manually adjusted for PI controllers, which can take time and require skill. Under different load circumstances, this strategy might not be the best one, which could result in performance issues. As was previously said, fuzzy control and ANN control successfully reduce error by fine-tuning membership functions (fuzzy) or training algorithms (ANN). By using an ANN to learn the behaviour of the system and automatically modify PI gains, the ANN-PI minimizes the need for user intervention. The Fuzzy granular provides self-tuning based on system dynamics by fusing sliding mode control [22] and fuzzy logic. The supplied figures (Figs. 15, 16) show how well each controller reduces current harmonics (as determined by THD). When compared to no compensation (7.46% THD), the PI controller provides a slight improvement (3.02% THD). The THD, ANN-PI (2.99%), and fuzzy granular (1.56%) are all much lower with the advanced controllers, and the fuzzy granular is particularly successful. With PI controller, THD decreases in a manner similar to that of source current THD (4.01% vs. 15.32% without DSTATCOM). Fuzzy-granular (2.37%) and ANN-PI (3.62%) are much lower for advanced controllers. It is clear that the fuzzy granular is very good at obtaining near-sinusoidal load currents because it shows the largest error reduction (THD reduction) for load current.

**Table 3:** System Specifications

| Parameter | value |
|---|---|
| Source | 100V,50HZ |
| Line impedance | 0.1Ω+j0.15mH |
| DSTATCOM | 0.001 Ω, 2.15 mH, 1 µF |
| VSC hysteresis controller band | 0.01 A |
| DC Capacitor | 9400 µF ,700V |
| Non-linear load | 60 Ω,30mH |
| Base power of the electrical generato | 3.88KW |
| Wind speed | 12m/s |
| Stator phase resistance | 2.2Ω |
| Stator phase inductance | 0.89 mH |

**Table 4:** Comparison table for harmonics

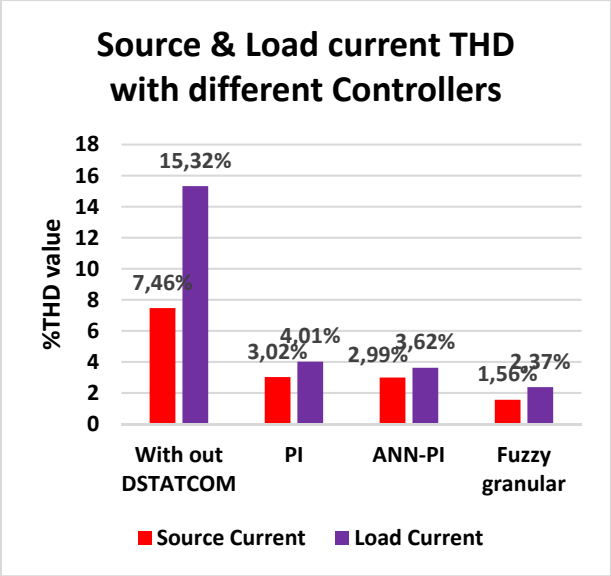


## 5. CONCLUSIONS

This work proposes a new topology and control strategy for the DSTATCOM with PMSG-WECS and BESS to compensate for the source and load side disturbances with decrease of THD and improvement of power factor. Fuzzy control systems, ANN-PI, and Fuzzy granular controlled with an active current component are used in the MPPT control scheme for the wind PMSG and DSTATCOM. The dc-link voltage shared by the DSTATCOM, PMSG, and BESS is enhanced by the PMSG WECS, which also filters and stores distorted current in a capacitor before pumping it back into the system as compensatory current. We have assessed the designed DSTATCOM-PMSG-WECS system through simulations using nonlinear load situations. The outcomes show how well the system worked to enhance the following aspects of electricity quality. By a large margin, the technology lowers the output voltage's THD to levels within IEEE standards-acceptable bounds. By doing this, harmonic currents are reduced, which lessens the possibility of voltage waveform distortion and poor power quality for other grid-connected equipment. The power factor is improved to almost unity by the DSTATCOM-PMSG-WECS system. In order to minimize energy waste and increase overall system efficiency, an optimum power factor indicates that the majority of the given power is being used for actual work. With a quick settling period, the technology keeps the DC-link voltage steady. This promotes overall system stability and guarantees

steady energy transfer within the DSTATCOM. Even in the midst of fleeting grid events, the DSTATCOM-PMSG-WECS with controllers supplies a clean and dependable power supply to the load.

## REFERENCES


[1] P. S. Sanjan et al., "Enhancement of Power Quality in Domestic Loads Using Harmonic Filters," in IEEE Access, vol. 8, pp. 197730-197744, 2020, doi: 10.1109/ACCESS.2020.3034734.

[2] S. R. Arya, B. Singh, R. Niwas, A. Chandra and K. Al-Haddad, "Power Quality Enhancement Using DSTATCOM in Distributed Power Generation System," in IEEE Transactions on Industry Applications, vol. 52, no. 6, pp. 5203-5212, Nov.-Dec. 2016, doi: 10.1109/TIA.2016.2600644.

[3] H. Fathy Mohamed, N. Hassan Saad and K. A. A. Salah Eldin, "Moderation of Voltage Sag and Swell in Grid Connected Wind Energy Based PMSG by DSTATCOM," 2018 Twentieth International Middle East Power Systems Conference (MEPCON), Cairo, Egypt, 2018, pp. 433-439, doi: 10.1109/MEPCON.2018.8635239.

[4] R. C. Portillo et al., "Modeling Strategy for Back-to-Back Three-Level Converters Applied to High-Power Wind Turbines," in IEEE Transactions on Industrial Electronics, vol. 53, no. 5, pp. 1483-1491, Oct. 2006, doi: 10.1109/TIE.2006.882025.

[5] P. A. Afsher, M. V. Manoj Kumar, C. M. Nirmal Mukundan and K. Shyju, "A PV-DSTATCOM With Adaptive DC-Link Voltage for Grid Integration and PQ Enhancement," in IEEE Transactions on Industry Applications, vol. 58, no. 5, pp. 6471-6484, Sept.-Oct. 2022, doi: 10.1109/TIA.2022.3182641.

[6] Hussain, Jawad, Mujahid Hussain, Safdar Raza, and Muhammad Siddique. "Power quality improvement of grid connected wind energy system using DSTATCOM-BESS." International Journal of Renewable Energy Research 9, no. 3 (2019): 1388-1397. https://doi.org/10.20508/ijrer.v9i3.9802.g7717

[7] Gallegos, Jimmy, Paul Arévalo, Christian Montaleza, and Francisco Jurado. "Sustainable Electrification—Advances and Challenges in Electrical-Distribution Networks: A Review." Sustainability 16, no. 2 (2024): 698. https://doi.org/10.3390/su16020698

[8] Thangella, Rajesh, Srinivasa Rao Yarlagadda, and Joseph Sanam. "Optimal power quality improvement in a hybrid fuzzy-sliding mode MPPT control-based solar PV and BESS with UPQC." International Journal of Dynamics and Control 11, no. 4 (2023): 1823-1843. 11. 10.1007/s40435-022-01095-0.

[9] Dearth, Manoj K., and Shreeram Choudhury. "Artificial neural network tuned PID controller for LFC investigation including distributed generation." International Journal of Numerical Modelling: Electronic Networks, Devices and Fields 33, no. 5 (2020): e2740. https://doi.org/10.1002/jnm.2740

[10] P. v. Ramana and K. M. Rosalina, "Power Quality Assessment of Distribution System Integrated with Wind Turbine Connected SRF-Controlled DSTATCOM," 2024 Second International Conference on Emerging Trends in Information Technology and Engineering (ICETITE), Vellore, India, 2024, pp. 1-6, doi: 10.1109/ic-ETITE58242.2024.10493683.

[11] S. B. Pandu et al., "Power Quality Enhancement in Sensitive Local Distribution Grid Using Interval Type-II Fuzzy Logic Controlled DSTATCOM," in IEEE Access, vol. 9, pp. 59888-59899, 2021, doi: 10.1109/ACCESS.2021.3072865.

[12] T. Ahmed, A. Waqar, R. M. Elavarasan, J. Imtiaz, M. Premkumar and U. Subramaniam, "Analysis of Fractional Order Sliding Mode Control in a D-STATCOM Integrated Power Distribution System," in IEEE Access, vol. 9, pp. 70337-70352, 2021, doi: 10.1109/ACCESS.2021.3078608.

[13] H. Li, J. Yang and W. Lu, "Design and Simulation Application of Fuzzy Controller Based on Granular Computing," *2022 7th International Conference on Computational Intelligence and Applications (ICCIA)*, Nanjing, China, 2022, pp. 256-261, doi: 10.1109/ICCIA55271.2022.9828430.

[14] S. Mangalapuri and V. S. S. Polamraju, "Enhance quality of Power in Grid Tie Solar Photovoltaic System using Deep learning MPPT," 2024 Second International Conference on Emerging Trends in Information Technology and Engineering (ICETITE), Vellore, India, 2024, pp. 1-6, doi: 10.1109/ic-ETITE58242.2024.10493635.

[15] Myla, A.K., Gorantla, S.R. (2023). Performance analysis of balanced integrated standalone microgrid under dynamic load conditions. Journal of New Materials for Electrochemical Systems, Vol. 26, No. 3,pp.155-163. https://doi.org/10.14447/jnmes.v26i3.a03

[16] Balram, G., Kumar, P.S. (2023). Harmonics reduction and balanced transition in hybrid renewable energy sources in a micro grid power system. Journal of New Materials for Electrochemical Systems, Vol. 26, No. 4, pp. 233-242. https://doi.org/10.14447/jnmes.v26i4.a01

[17] Kotla, R.W., Yarlagadda, S.R. (2022). Real-time simulations on ultracapacitor based UPQC for the power quality improvement in the microgrid. Journal of New Materials for Electrochemical Systems, Vol. 24., No. 3, pp. 166-174. https://doi.org/10.14447/jnmes.v24i3.a04

[18] Kumar, N.B., Rao, M.U.M., Veeranjaneyulu, J., Chandra, B.M., Venkatesh, P.M. (2024). An optimized superconducting magnetic energy storage for grid connected systems. Journal of New Materials for Electrochemical Systems, Vol. 27, No. 1, pp. 52-59. https://doi.org/10.14447/jnmes.v27i1.a08

[19] Li Fu, Xiuwei Fu, Ping Yang (2021). Maximum Power Point Tracking in Solar Cells with Power Quality Preservation Based on Impedance Matching Concept for Satellite Electrical Energy Supply, Journal of New Materials for Electrochemical Systems Vol. 24, No.2, April 2021, pp.111-119 https://doi.org/10.14447/jnmes.v24i2.a08

[20] Vigneshwaran, P., Padmavathi, N., Nirmala, G., Sowmiya, A. (2022). An intelligent cooling system

based on predictive time domain algorithm with thermoelectric coolers for wind turbines. Journal of New Materials for Electrochemical Systems, Vol. 25, No.2, pp. 142-144. https://doi.org/10.14447/jnmes.v25i2.a08

[21] Riquelme, J.A., Sebastian, P.J., Gamboa, S.A., Campos, J. (2018). Design and development of a real-time characterization system for energy conversion devices. Journal of New Materials for Electrochemical Systems, Vol. 21, No. 1, pp. 7-13. https://doi.org/10.14447/jnmes.v21i1.515

[22] Assam, B., Sabir, M., Abdelghani, H. (2020). Modeling and control of power system containing PV system and SMES using sliding mode and field control strategy. Journal of New Materials for Electrochemical Systems, Vol. 23, No. 3, pp. 190-197. https://doi.org/10.14447/jnmes.v23i3.a06

[23] Subrahmanyam, K.V., Rosalina, K.M. (2024). The impact of functionally graded material insulator in a three phase gas insulated busduct under protrusion defect. Journal of New Materials for Electrochemical Systems, Vol. 27, No. 1, pp. 16-24. https://doi.org/10.14447/jnmes.v27i1.a03

[24] Dharmasa, Ambikapathy, A., Rao, M.U.M., Rao, G.S. (2023). Development of matrix based single equation to compute OC-SC tests parameters for 1-Phase transformer. Journal of New Materials for Electrochemical Systems, Vol. 26, No. 4, pp. 243-247. https://doi.org/10.14447/jnmes.v26i4.a02

[25] Koley, I., Datta, A., Panda, G.K. (2023). Load frequency control in renewable energy penetrated hybrid power systems. Journal of New Materials for Electrochemical Systems, Vol. 26, No. 4, pp. 268-276. https://doi.org/10.14447/jnmes.v26i4.a05

[26] S. Mopidevi, K. S. Dasari, et al," Design, control and performance comparison of PI and ANFIS controllers for BLDC motor driven electric vehicles"Measurements: SensorsVol31,2024,https://doi.org/10.1016/j.measen.2023.101001

[27] Subrahmanyam, K.V., Rosalina, K.M. Electric field intensity minimization in three-phase gas-insulated busduct with metal inserts under delamination. Int J Adv Manuf Technol (2023). https://doi.org/10.1007/s00170-023-12867-z